Materials Horizons

ROYAL SOCIETY OF CHEMISTRY

COMMUNICATION

View Article Online
View Journal | View Issue

Cite this: *Mater. Horiz.*, 2021, 8, 1561

Received 2nd January 2021,
Accepted 11th March 2021

DOI: 10.1039/d1mh00004g

rsc.li/materials-horizons

The transfer and amplification of cyanostilbene molecular function to advanced flexible optical paints through self-crosslinkable side-chain liquid crystal polysiloxanes†

Jahyeon Koo,[a] Junhwa Jang,[a] Seok-In Lim,[a] Mintaek Oh,[a] Kyung Min Lee,[b] Michael E. McConney,[b] Luciano De Sio,[c] Dae-Yoon Kim*[d] and Kwang-Un Jeong *[a]

A self-crosslinkable side-chain liquid crystal polysiloxane containing cyanostilbene (Si–CSM) was newly synthesized for the development of a new generation of flexible optical paints. The photoisomerization of the cyanostilbene moiety at the molecular level was transferred and amplified to the phase transition of Si–CSM, resulting in changes in the macroscopic optical properties of the Si–CSM thin film. The self-crosslinking reaction between Si–H groups in the Si–CSM polymer backbone caused the self-crosslinked Si–CSM thin film to be very elastic and both thermally and chemically stable. Therefore, the self-crosslinked Si–CSM thin film endured stretching and bending deformations under relatively harsh conditions. In addition, the uniaxially oriented and self-crosslinked Si–CSM thin film generated linearly polarized light emission. Polarization-dependent and photopatternable secret coatings were fabricated *via* a spontaneous self-crosslinking reaction after coating the Si–CSM paint and irradiating ultraviolet (UV) light through a photomask. This newly developed flexible optical Si–CSM paint can be applied in next-generation optical coatings.

New concepts

Stimuli-induced color and luminescence tunable organic materials have been extensively studied for advanced optical applications. Among them, photoisomerizable dyes are attracting significant attention because of their advantages such as remote switching and photopatterning. However, the photoisomerization accompanying a large volume change is occasionally suppressed in the solid state or at room temperature. Thus, to improve their practicality, the applicability range of photoisomerizable dyes needs to be further extended to all cases, including polymer network systems. Herein, we present a reasonable strategy to solve this issue through the introduction of polymethylhydrosiloxane (PMHS). The newly synthesized side-chain liquid crystal polysiloxane (Si–CSM) for advanced optical paints consists of a PMHS backbone and cyanostilbene side chain. The flexibility of the PMHS backbone induces the formation of a liquid crystal phase over a wide temperature range, which facilitates both photoisomerization and uniaxial orientation at room temperature. In addition, Si–CSM can be self-crosslinked without any crosslinker in the presence of a small amount of Pt catalyst. Therefore, simplification of the paint composition and robustness of the Si–CSM optical paint are simultaneously achieved. The self-crosslinked Si–CSM paint shows enhanced thermal and chemical stability and can be bent and stretched under relatively harsh conditions. Consequently, polarization-dependent and photopatternable secret coatings for flexible objects are successfully demonstrated through photo-isomerization and subsequent self-crosslinking processes.

Introduction

Color and luminescence are studied because visual elements play a critical role in delivering information and intuitive communication. Thus, many types of materials with various colors and emission properties are becoming increasingly interesting research topics. Inorganic pigments and organic dyes, including metal-complex hybrids, have been synthesized and modified with the introduction of various chromophores and substituents to obtain desired high-performance colors.[1–5] In particular, multicolor properties that can be adjusted in a single molecule are attracting attention as advanced optical applications. By applying external stimuli such as thermal energy, vapor, light, pressure and electric field, the energy level of molecules with multicolor properties can be dynamically controlled.[6–10] These external stimuli induce different molecular packing, chemical reactions, phase transitions, and oxidation–reduction, resulting in a variation in molecular energy levels and optical properties.

[a] *Department of Polymer-Nano Science and Technology, Department of Nano Convergence Engineering, Jeonbuk National University, Jeonju 54896, Republic of Korea. E-mail: kujeong@jbnu.ac.kr*
[b] *US Air Force Research Laboratory, Wright-Patterson Air Force Base, Ohio 45433, USA*
[c] *Center for Biophotonics and Department of Medico-Surgical Science and Biotechnologies, Sapienza University of Rome, Latina 04100, Italy*
[d] *Functional Composite Materials Research Center, Korea Institute of Science and Technology, Jeonbuk 55324, Republic of Korea. E-mail: kdaeyoon@kist.re.kr*

† Electronic supplementary information (ESI) available. See DOI: 10.1039/d1mh00004g

Photoisomerization of organic dyes and luminogens is an effective and unique way to change both their color and luminescence. Light-induced conformational changes in photoisomerizable moieties can induce dynamic changes in the molecular energy system and the phase transition, which affect their macroscopic optical property.[11–13] Furthermore, remote-controllable patterning in specific areas can be performed by irradiating light through a photomask.[12,14,15] However, to date, these advantages have not been exploited, especially in polymer network systems. Complex molecular design and formulation are inevitable to achieve both optical changes by photoisomerization and polymer stabilization. In addition, strong molecular packing in the solid state and low molecular mobility at room temperature occasionally suppress photoisomerization.[16] Particularly, photoisomerization requiring a large volume change is more restricted in the solid state. However, for the advanced practical application of photoisomerizable luminogens, these limitations must be overcome.

Herein, we introduce a new strategy for the development of advanced flexible optical paints (Scheme 1). The flexible optical paint was newly prepared by mixing a self-crosslinkable side-chain liquid crystal polysiloxane containing cyanostilbene (abbreviated as Si–CSM), Karstedt's catalyst, and 1-ethynyl-1-cycolhexanol (inhibitor) with an organic solvent. The newly synthesized Si–CSM consists of polymethylhydrosiloxane (PMHS) as the backbone, partially substituted cyanostilbene side chains, and residual Si–H groups in its backbone. Considering that the cyanostilbene moiety in the side chain is a representative aggregation-induced emission (AIE) luminogen, Si–CSM shows strong emission in the solid state. In addition, the photoisomerization of the cyanostilbene moiety at the molecular level can be transferred and amplified to induce a phase transition in Si–CSM, which results in changes in the macroscopic optical properties of the Si–CSM thin film. The residual Si–H groups remaining after partial substitution of the side chains can react with each other in the presence of very small amounts of a platinum catalyst, such as Karstedt's catalyst. This one-component, self-crosslinking reaction significantly enhances the chemical, thermal and mechanical stability of the self-crosslinked Si–CSM thin film. The flexibility of the polysiloxane backbone not only contributes to the elastomeric mechanical properties of the self-crosslinked Si–CSM, but also allows it to have a liquid crystal (LC) phase over a wide temperature range. Additionally, the photoisomerization of Si–CSM can occur at room temperature without any difficulty, and the uniaxial molecular orientation is also easily induced by mechanical shear. A small amount of inhibitor in the Si–CSM paint prevents undesirable crosslinking reactions before the coating and photopatterning process. Different solvent concentrations were used to achieve the desired viscosity for each coating process. Taken together, light-induced optical changes, and photo-patternable and polarized emissive optical coatings can be realized *via* the sequential process of Si–CSM paint coating, ultraviolet (UV) light irradiation through a photomask, and spontaneous crosslinking by the self-crosslinking reaction.

Results and discussion

A programmed side-chain liquid crystal polysiloxane (abbreviated as Si–CSM) for application in advanced flexible optical paint was newly synthesized through the hydrosilylation reaction between the silicon hydride group of polymethylhydrosiloxane (PMHS) and a vinyl-functionalized luminogenic cyanostilbene side chain (CSM). The detailed synthetic procedures for Si–CSM and its intermediates are described in the (Fig. S1, ESI†). The successful synthesis and purity of these compounds were confirmed through proton (^{1}H), and carbon (^{13}C) NMR (Fig. S2–S5, ESI†). After the catalytic hydrosilylation reaction between PMHS and CSM, a new peak corresponding to Si–CH_2–C appeared at 0.60 ppm, indicating that PMHS is chemically linked with CSM (Fig. S6, ESI†). Conversely, the peak corresponding to the vinyl group of CSM disappeared completely in the ^{1}H-NMR spectrum.[17,18] The unreacted

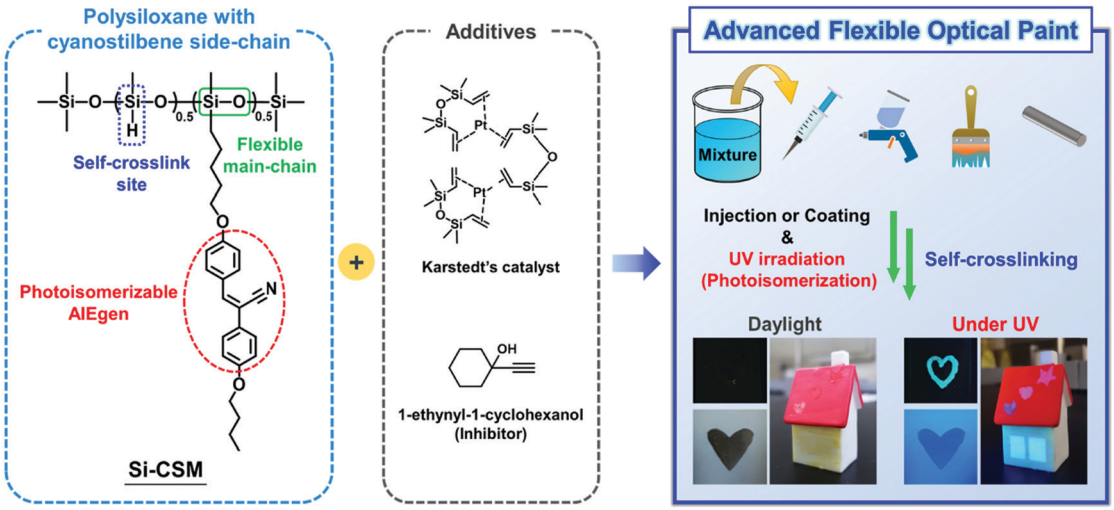

Scheme 1 Schematic illustration of the programmed Si–CSM and its application in advanced flexible optical paint.

Si–H groups observed at 4.74 ppm were purposely left for self-crosslinking reaction and can be used to stabilize Si–CSM against external stimuli. The molar ratio of the self-crosslinking site to the photoisomerizable AIEgen was about 1 : 1. The molecular weight of Si–CSM measured by gel permeation chromatography (GPC) was 10 035 g mol^{-1} (Fig. S7, ESI†), which is similar to the estimated value (9680 g mol^{-1}) calculated from the ^{1}H-NMR spectrum of Si–CSM. In the FT-IR spectrum of Si–CSM, the characteristic stretching bands of the C≡N and Si–H groups were observed at 2211 and 2165 cm^{-1}, respectively (Fig. S8, ESI†).[19,20]

The phase transition behaviors of Si–CSM were monitored by polarized optical microscopy (POM) at different temperatures (Fig. 1a) and differential scanning calorimetry (DSC) at different scanning rates (Fig. 1b). The endothermic peak at about 120 °C in the heating trace of the DSC thermograms indicates a first-order phase transition between the isotropic and mesomorphic state.[21,22] The step change in heat capacity detected at around 10 °C is attributed to the glass transition temperature (T_g) of Si–CSM. The low T_g of Si–CSM is mainly due to the flexible PMHS backbone. The phase transformations were further supported by the morphological observation on the micrometer length scale. On cooling at 5 °C min^{-1} from the isotropic liquid state, an optical texture with strong birefringence was formed against the dark state, suggesting the emergence of a low-ordered liquid crystal (LC) phase. There was no noticeable change in the texture until the sample temperature was elevated above 120 °C again starting from room temperature. The LC mesophase was maintained over a wide temperature range of 8 °C to 120 °C.[23] Additionally, the thermal degradation temperature of Si–CSM was 392 °C, which was determined by thermogravimetric analysis (TGA) (Fig. S9, ESI†).

To investigate the self-assembly behavior of Si–CSM in detail, one-dimensional (1D) wide-angle X-ray diffraction (WAXD) patterns were obtained under different annealing conditions. As can be seen in Fig. S10 (ESI†), the two amorphous halos at 130 °C indicate the amorphous nature of Si–CSM. The incoherent scattering between the PMHS backbones led to the broad halo at 2θ = 10.60° (d = 0.83 nm).[24,25] The average distance of 0.44 nm (2θ = 20.05°) originated from the short range positional order between the cyanostilbene luminogens. When the temperature decreased from 130 °C to 110 °C, the broad scattering halo in the range 2θ = 15° ∼ 25° suddenly shifted to 2θ = 21.13° (d = 0.42 nm), while the weak halo at 2θ = 10.60° remained in the same region. A new single diffraction peak concurrently emerged at 2θ = 6.34° (d = 1.39 nm). Considering the first-order peak with a very low intensity and no second-order peak, Si–CSM has a low-ordered smectic A (SmA) LC phase.[25,26] In addition, the calculated layer distance is much smaller than the side-chain length (l = 2.5 nm) of Si–CSM because of side-chain interdigitation.[25,26]

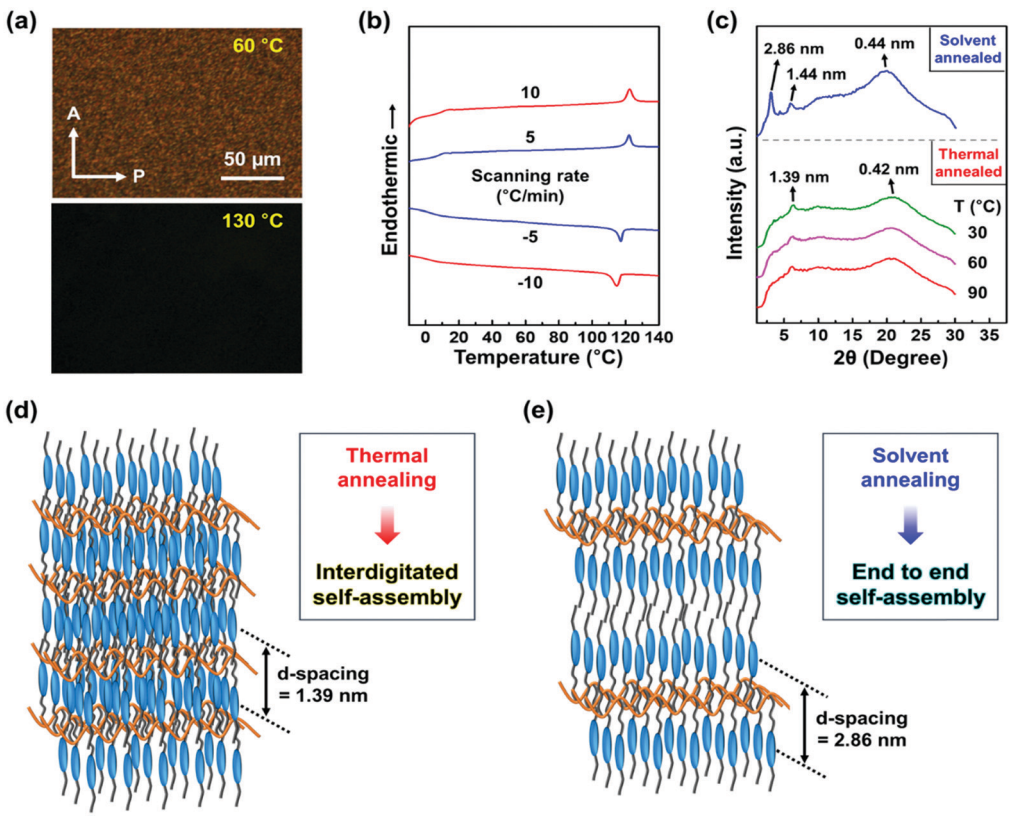

Fig. 1 Phase transition behaviors of Si–CSM: (a) POM textures at different temperatures, (b) DSC thermograms at different scanning rates, (c) 1D WAXD patterns obtained by different annealing processes, and schematic illustrations of the self-assembled structures obtained by (d) thermal and (e) solvent annealing process.

Given that the thermal transition behaviors depending on the rate of heating and cooling can be related with the phase transformation kinetics, isothermal annealing experiments were conducted. Si–CSM in the isotropic phase was cooled to a temperature of 90 °C, 60 °C, and 30 °C at a rate of 5 °C min^{-1}, and then isothermally annealed at that temperature for 60 min. However, there was no change in the 1D WAXD patterns annealed isothermally at these temperatures and the above-mentioned time range, as shown in Fig. 1c. This indicates that Si–CSM shows a LC phase formed directly from the isotropic state over the wide temperature range of 8 °C to 120 °C.

Si–CSM subjected to 2 days of solvent annealing in a good solvent of chloroform exhibited multiple reflections (Fig. 1c). The peaks in the low-angle region were separated by two 2θ values, indicating a lamellar structure. The primary reflection observed at $2\theta = 3.08^{\circ}$ corresponds to the interlayer spacing (L) between lamellae of approximately 2.86 nm. These reflections indicate that a sublayer was only observed in the solvent-annealed Si–CSM (form II, Fig. 1e), but not in the thermally annealed Si–CSM (form I, Fig. 1d). The average lateral distance of the side-chain was 0.44 nm ($2\theta = 20.03^{\circ}$). The long-term solvent annealing in a good solvent can increase the chain mobility, yielding an improvement in the recognition of nanophase-separated building blocks.[27–29] It should be noted that the phase transition between form I and II was reversible and could be repeated several cycles (Fig. S11, ESI†). The reversible changes in the layer spacing between 1.39 nm and 2.86 nm during the phase transition cycle by applying heat and solvent treatment were extracted by 1D WAXD. The driving force for the phase transition is due to the stability difference upon thermal or solvent annealing. Form I of Si–CSM was thermodynamically stable at a temperature below the isotropic state, while form II was caused by cooperative interactions with the solvent. Thus, Si–CSM exhibited structural changes depending on the processing history. The thermally annealed Si–CSM showed smectic domains with interdigitated molecular packing. The solvent-annealed sample exhibited layer structures with end-to-end self-assembly by minimized overlapping of the extended butyl side chain.[29–31]

The bulk density of this LC polymer can further account for the two different molecular packing modes (Fig. S12, ESI†). The density of form I and II was measured to be 1.11 g cm^{-3} and 1.08 g cm^{-3}, respectively. The thermally annealed Si–CSM possessed a slightly higher density than the solvent-annealed Si–CSM. The monolayer structure with a layer thickness of 1.39 nm can contain more side-chain molecules than the bilayer structure with a layer thickness of 2.86 nm under the same volume of macroscopic pieces owing to the compact molecular packing. The proposed molecular packing models of Si–CSM obtained in the different annealing processes are schematically illustrated in Fig. 1d and e.

The aggregation-induced emission (AIE) properties of Si–CSM were investigated by ultraviolet-visible (UV-Vis) and photoluminescence (PL) spectrophotometry. Several Si–CSM solutions with different water fractions (f_w) in the range of 0 to 90 were prepared, and then their absorption and PL changes were monitored (Fig. S13, ESI†). The dissolved Si–CSM in tetrahydrofuran (THF) showed an absorption band at 348 nm, corresponding to the cyanostilbene moiety. By adding a large amount of water as a poor solvent, the transparent Si–CSM solution turned cloudy due to molecular aggregation, resulting in light scattering. The absorption band was red-shifted from 348 nm to 369 nm and broadened by J-aggregation of the cyanostilbene moieties in Si–CSM.[32,33] The emission band shifted gradually to a longer wavelength and the intensity increased with an increase in f_w (Fig. 2a and Fig. S13, ESI†). The PL intensity of Si–CSM increased slowly in the aqueous mixtures when $f_w < 0.5$, while it increased dramatically when $f_w > 0.5$. Obviously, a change in the absorption band and greatly enhanced emission of Si–CSM by aggregation were observed. Compared to the Si–CSM solution, the thin solid films also showed much stronger emission at λ_{max} = 462 nm (Fig. 2b). The thin films of Si–CSM prepared by thermal or solvent annealing process exhibited different layer-spacings in their self-assembled structures, but their emission spectra were almost identical. This indicates that the intermolecular interactions between the cyanostilbene luminogens, which mainly affect the emission properties, do not change significantly within the layer. It should be noted that the d-spacing of the cyanostilbene luminogens in the thermally annealed and solvent-annealed Si–CSM samples was 0.42 nm and 0.44 nm, respectively.

The photoisomerization of the cyanostilbene group in Si–CSM was studied using ^{1}H-NMR, UV-Vis and PL measurements. After UV irradiation (365 nm wavelength, 10 mW cm^{-2}) of Si–CSM dissolved in deuterochloroform for 15 min, two new peaks appeared at 7.13 and 6.65 ppm in the ^{1}H-NMR spectrum (Fig. S14, ESI†). These two peaks (H_a' and H_b') correspond to the proton of the double bond and the aromatic ring in the *cis*-cyanostilbene, respectively, and the peak at 3.83 ppm corresponds to the proton at the H_c' position.[12,34,35] After UV irradiation under previous conditions, the absorption band of the Si–CSM solution shifted to a shorter wavelength (Fig. S15a, ESI†). This blue-shift phenomenon can be explained by the photoisomerization of the cyanostilbene group from the trans to cis isomer, resulting in a shorter conjugation length in the luminogen.[12,34,35] As shown in Fig. S15b (ESI†), a blue-shifted emission at 390 nm was also induced. The enhanced emission efficiency is attributed to the restricted molecular rotational motion of the relatively rigid *cis* isomer.[36,37]

The photoisomerization behavior was also observed in the Si–CSM solid films. The optical changes in the transmittance and PL spectra upon UV irradiation are presented in Fig. 2c and d, respectively. The solid film before UV irradiation showed low transmittance due to the light scattering from the micrometer-sized multi-domain. Particularly, the low transmittance at wavelengths below 500 nm is caused by the absorption of the self-assembled Si–CSM. After UV irradiation, the transmittance in the visible wavelength range rapidly increased to more than 80%. The phase transition from the smectic phase to the isotropic state is driven by photoisomerization, which results in the formation of a macro-sized single domain and high

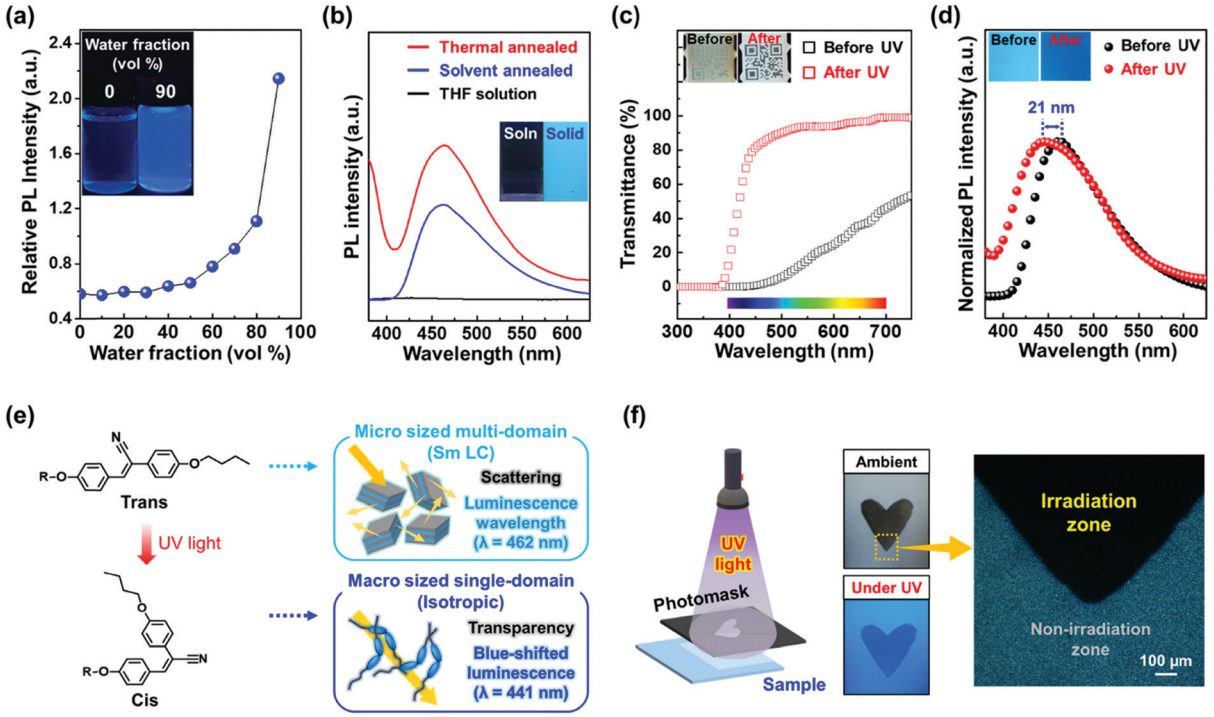

Fig. 2 Aggregation-induced emission and optical changes upon photoisomerization of Si–CSM: (a) PL intensity of Si–CSM solution (0.005% (w/v), THF/H_2O) with different water fractions, (b) PL spectra of Si–CSM solution and solid films, (c) transmittance and (d) PL spectra changes in Si–CSM film (thickness: 30 μm) before and after UV irradiation, (e) schematic illustration of the optical changes upon photoisomerization, and (f) photopatterned heart-shaped sample and the corresponding POM texture.

transmittance in the Si–CSM solid film.[13,38] As can be seen from the inset in Fig. 2c, the image of the QR code can be seen through the transparent Si–CSM film. In addition, the blue-shifted absorption of cis isomer contributes largely to the transmittance enhancement at a wavelength in the range of 400 to 500 nm. The emission peak of the solid film shifted from 462 to 441 nm under UV irradiation, and the 21 nm blue shift in the emission peak showed the change in luminescent color, as shown in the inset of Fig. 2d. The PL quantum yield of the initial and photoisomerized Si–CSM was measured to be 1.01% and 1.37%, respectively (Fig. S16, ESI†). Thus, there was no significant change in quantum yield. In summary, the photoisomerization of solid-state Si–CSM can occur easily at room temperature upon exposure to UV light and can be accompanied by optical changes in both transmittance and luminescence (Fig. 2e). Based on these characteristics, the Si–CSM films could be successfully photopatterned using a photomask. As showed in Fig. 2f, the heart-shaped pattern shows a great contrast between the exposed and unexposed area. The exposed area is transparent and has a blue-shifted emission under UV light. The difference between the exposed and unexposed area was also observed in the POM images. Unlike the bright textures of the unexposed area, the exposed area showed no birefringence, indicating the isotropic state of Si–CSM.

To prepare the Si–CSM optical paint, Si–CSM was mixed with a very small amount of platinum(0)-1,3-divinyl-1,1,3,3-tetramethyl-disiloxane complex solution (Karstedt's catalyst, in xylene, Pt ~ 2%) and 1-ethynyl-1-cyclohexanol (inhibitor). The mixture composition is shown in Fig. 3a and the detailed preparation is described in the ESI.† The prepared Si–CSM mixture was slowly cured by the self-crosslinking reaction between the Si–H groups on the polymer backbone. At room temperature, it took several days for the paint to be fully cured. Thus, to reduce the curing time, the painted film was first cured at room temperature for 12 h and then kept at 60 °C for 12 h.[39,40] The crosslinking density of the film could be controlled by the amount of catalyst (Fig. S17, ESI†). There was no significant change in the LC and optical properties depending on the crosslinking density under the given conditions (Fig. S18, ESI†). The fully cured film exhibited a very smooth surface and showed a root mean square (RMS) roughness of 7.93 nm (Fig. S19, ESI†). With the Si–CSM paint, light-induced secret and photopatterned coatings could be easily prepared by painting, subsequent UV irradiation (transition to secret mode and photopatterning) and spontaneous curing through self-crosslinking reaction (Fig. 3d).

During the self-curing process, Si–Si and Si–O–Si crosslink bonds are created (Fig. 3c). The protons in the backbone are detached by Pt in the catalyst and Si–Si bonds are formed (dehydrocoupling). Then, H and Si radicals are formed by homolytic cleavage of the Si–H bonds and the generated H_2 gas forms Si–O–Si bonds in the presence of O_2 gas (oxidation).[39,40] In the ^{29}Si-NMR spectrum shown in Fig. 3b, the Si–O–Si bonds are detected as two peaks located at −56 and −66 ppm. It is difficult to find Si–Si bonds at −20 ppm because of the overlap with the Si atoms in the Si–R bonds.[39,40]

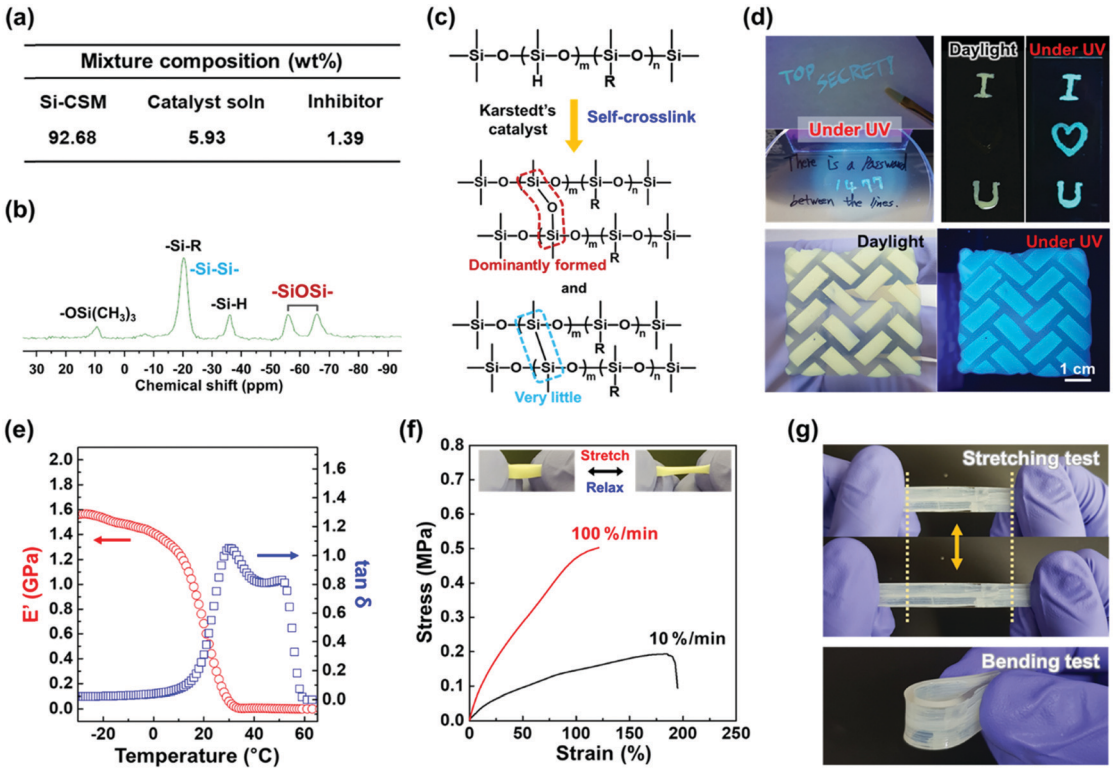

Fig. 3 Self-crosslinkable Si–CSM paint and its mechanical properties: (a) mixture composition of the well-formulated Si–CSM paint, (b) solid-state ^{29}Si-NMR spectrum of the self-crosslinked Si–CSM paint, (c) schematic diagram of the self-crosslinking reaction, (d) photographs of secret and patterned coatings using the Si–CSM paint, (e) DMA graph of the self-crosslinked Si–CSM film, (f) strain-stress curves of the self-crosslinked film at different strain rates, and (g) simple mechanical tests of the Si–CSM paint (thickness: 50 μm) coated on PDMS.

However, the presence of Si–Si bonds was confirmed in the ^{29}Si-NMR spectrum of the self-crosslinked PMHS (Fig. S20, ESI†). The Si–Si bond at −20 ppm was clearly observed due to the absence of Si–R bonds in PMHS. Referring to Fig. 3b, the unreacted Si–H groups after self-crosslinking are observed at −36 ppm. Considering the integration of the respective peaks in the spectrum, the Si–O–Si bond was dominantly formed. This may be related to the self-crosslinking mechanism and reaction kinetics. The crosslinking of the self-crosslinked film was further confirmed by its enhanced thermal stability and chemical resistance. The self-crosslinked Si–CSM paint film did not flow at 180 °C, which is much higher than the melting point (120 °C) of Si–CSM (Fig. S21a and b, ESI†). The thermal degradation of the self-crosslinked film began to occur above 363 °C, as shown in Fig. S21c (ESI†). The crosslinked Si–CSM paint started to decompose at a temperature slightly below the degradation point of pure Si–CSM because the Si–CSM paint contains a small amount of additives including catalyst and inhibitor.[41] After removing these impurities with acetone, the degradation temperature of the crosslinked film increased to 379 °C. The self-crosslinked film did not dissolve after rinsing with chloroform or immersion in acetone for 30 min (Fig. S22, ESI†). Due to the self-crosslinking, the Si–CSM paint film could retain its shape at high temperature and against chemical attack.

The mechanical properties of the self-crosslinked Si–CSM films were examined by dynamic mechanical analysis (DMA) and tensile tests. As shown in Fig. 3e, the storage modulus in the glassy state below 0 °C is above 1.4 GPa. With an increase in temperature, the modulus decreased to tens of MPa above 10 °C, the T_g of the film. At around 55 °C, a further decrease in storage modulus occurred due to the phase transition from smectic to nematic LC phase.[42,43] Accordingly, the loss tangent (tan δ) exhibited two peaks at 29 °C and 53 °C. These results are in good agreement with the DSC and 1D WAXD data for the crosslinked film (Fig. S23, ESI†). In addition, the nematic to isotropic phase transition (T_{NI}) of the film occurred at 113 °C.

As shown in Fig. 3f, the self-crosslinked Si–CSM film showed that reversible stretching and relaxation behavior is possible within about 100% strain due to its partially crosslinked and flexible polysiloxane backbone. Under different strain rates of 10% min^{-1} and 100% min^{-1} at 25 °C, the film broke at 184% and 121% strain, and its tensile strength was 0.19 MPa and 0.50 MPa, respectively. The mechanical and fracture properties of most polymers depend on the applied strain rate due to their viscoelasticity.[44] Thus, based on its mechanical properties, Si–CSM paint can be coated and applied to flexible objects. As shown in Fig. 3g, the Si–CSM paint coated on a PDMS film showed stable stretching and bending behavior. It was not broken during several bending and stretching tests. Furthermore, undesirable changes in the emission color of the crosslinked Si–CSM during stretching and relaxing were not detected although it has been reported that some AIE luminogen-based

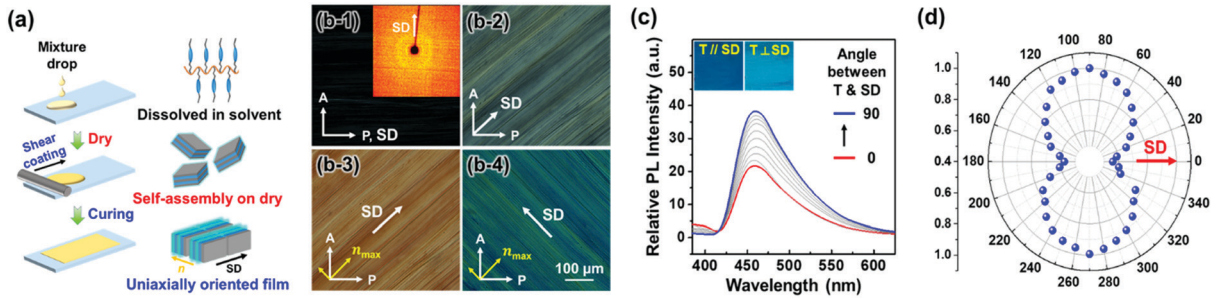

Fig. 4 Shear-induced uniaxially oriented Si–CSM coatings: (a) schematic illustration of shear-induced orientation, (b) POM observation with a retardation plate (inset figure is the 2D WAXD pattern of the oriented film), (c) polarized PL spectra, and (d) PL intensity as a function of the angle between shear direction (SD) and transmittance (*T*) axis of a polarizer.

polymers have mechanochromic properties (Fig. S24a, ESI†).[45,46] The emission spectra of the stretched and relaxed Si–CSM film exhibited almost the same PL spectra. As shown in Fig. S24b and c (ESI†), no distinct changes in the structure and orientation of the self-assembled structures were observed according to the POM and WAXD results. Therefore, the emission properties of the self-crosslinked Si–CSM paint were well-maintained under mechanical load, a beneficial phenomenon in terms of general painting applications.

Applying shear force to the drop-casted and dried Si–CSM paints yielded uniaxially oriented thin films, which was caused by the high molecular mobility of Si–CSM at room temperature (Fig. 4a). The oriented and subsequently cured film with a thickness of 20 μm was used for this study. As shown in Fig. 4b, the sheared sample showed birefringence as a function of the angle between shear direction (SD) and polarizer axis. Dark and maximum bright images were observed when the SD and polarizer axis were 0° and 45°, respectively, indicating that the self-assembled structure formed upon drying is uniaxially oriented by the shear force.[47] The 2D WAXD image in Fig. 4b-1 also supports the uniaxially oriented and self-assembled structure of the sheared Si–CSM paint. Given that Si–CSM was annealed by the solvent through the solution casting and drying process, first and second order diffractions were observed at the equator, indicating that the layer normal is perpendicular to the SD.[48,49] The molecular arrangement was further identified by POM observations with a 530 nm retardation plate (Fig. 4b-3 and b-4). When the SD and slow axis of the retardation plate were parallel, a yellowish POM image was observed due to the retardation subtraction.[47] When the SD and the slow axis were perpendicular, a blueish POM image appeared by the addition effect. Thus, it can be concluded that the long axis of cyanostilbene is perpendicular to the SD and layer.

Before measuring the linearly polarized emission property, the polarized absorption of the uniaxially oriented Si–CSM film was confirmed (Fig. S25, ESI†). The maximum absorption occurs in the perpendicular condition between the SD and transmittance axis (*T*) of the polarizer. Conversely, the minimum absorption spectrum is presented when SD and

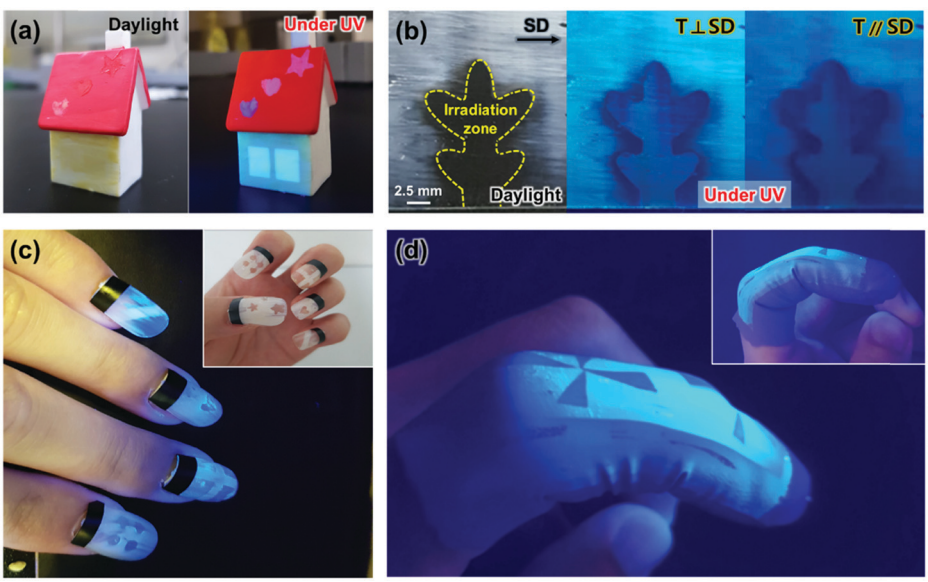

Fig. 5 Demonstration of the advanced flexible optical coatings using the Si–CSM paints: (a) decorated miniature house, (b) photopatterned and polarized emissive coating, and patterned (c) artificial nails and (d) rubber glove.

T are parallel. Similarly, the PL spectra of the uniaxially oriented Si–CSM film showed polarized emission behaviors (Fig. 4c and d). The PL intensity gradually increased as the angle between the SD and T increased from parallel (0°) to perpendicular (90°). The obvious contrast between the m'aximum and minimum intensity is shown in the inset of Fig. 4c. The calculated polarization ratio of $P = I_{\parallel}/I_{\perp}$ is 1.79 and the order parameter of $S = (I_{\parallel} - I_{\perp})/(I_{\parallel} + 2I_{\perp})$ is 0.21, where $I_{\parallel}$ and $I_{\perp}$ are the maximum PL intensities in the parallel and perpendicular conditions between SD and T, respectively.[41] The somewhat low P and S values may originate from some defects in the shear-coated Si–CSM paint and the attenuated orientational order caused by the self-crosslinking reaction.[50,51] It should be noted that the measured polarization ratio (P) of the shear coated film before the self-crosslinking reaction was 2.10 (Fig. S26, ESI†). However, the sufficiently different PL intensity according to the angle between SD and T can result in different optical signals in polarized paint applications.

Utilizing the light-induced optical change behavior, flexible mechanical properties, and shear-induced orientation of the Si–CSM paint, a variety of advanced flexible optical coatings was demonstrated. After painting and photopatterning in certain areas, the UV exposed areas were invisible under ambient light and showed a different luminescence color under UV light, as shown in Fig. 5a. Fig. 5c shows the programmed artificial nails fabricated with the Si–CSM paint. Polarized light-emissive coatings were also obtained by applying shear force to the drop casted and dried paint (Fig. 5b). Subsequent UV irradiation through a photomask also led to optical changes in certain areas and the UV exposed areas did not exhibit polarized emission properties due to the loss of molecular orientational order through photoisomerization. By combining shear-induced polarized emission and photo-patterning of transmittance and luminescence, dual-mode optical patterns could be easily realized with a polarizer. Furthermore, the Si–CSM paint can be applied to flexible objects because of its elastomeric properties. As shown in Fig. 5d, the painted and subsequently photopatterned nitrile glove displayed the programmed optical patterns. Furthermore, the paint on the glove was robust in both mechanical and optical properties during repetitive flexion and extension of a finger.

Conclusions

The programmed Si–CSM was newly synthesized for the development of advanced flexible optical paints. The Si–CSM film showed strong emission at 462 nm because of the AIE property of its cyanostilbene side chain. Because the flexible backbone of Si–CSM allowed the formation of a low-ordered smectic A (SmA) LC phase over a wide temperature range between 8 °C and 120 °C, Si–CSM could be easily photoisomerized and oriented even at room temperature. The UV-irradiated Si–CSM film exhibited a highly enhanced transmittance and blue-shifted emission at 441 nm due to the photoisomerization of the cyanostilbene moiety. The uniaxially oriented and self-crosslinked Si–CSM thin film emitted linearly polarized light. Also, the self-crosslinked Si–CSM thin film could be bent and stretched because of its high elasticity and strong mechanical stability, which resulted from the self-crosslinking reaction between the Si–H groups in the Si–CSM backbone. By combining the light-induced optical change behavior and shear-induced polarized emission property of the Si–CSM paint, photopatternable and polarized light emissive coatings were achieved. Thus, the proposed Si–CSM paint can be applied in security and advanced optical coatings for flexible objects and soft actuators.

Conflicts of interest

There are no conflicts to declare.

Acknowledgements

This work was supported by BRL Program (2020R1A4A1018259), Mid-Career Researcher Program (2021R1A2C2009423), Basic Science Research Program (NRF-2019R1A6A3A13092060) funded (2019R1A6A3A13092060), JBNU Fellow, Korea Government MSIT (2021R1R1R1004226), Technology Innovation Program (MOTIE20011317), Open Research Program of KIST (2E31332), Air Force Office of Scientific Research (FA8650-16-D-5404-0013, USA), and NATO Science for Peace and Security Program (G5759).

Notes and references

1 S. Jin, G. Cheng, G. Z. Chen and Z. Ji, *J. Porphyrins Phthalocyanines*, 2005, **9**, 32.
2 S. Redon, G. Eucat, M. Ipuy, E. Jeanneau, I. Gautier-Luneau, A. Ibanez, C. Andraud and Y. Bretonniere, *Dyes Pigm.*, 2018, **156**, 116.
3 B. K. Bera, C. Chakraborty and S. Malik, *J. Mater. Chem. C*, 2017, **5**, 6872.
4 A. Maron, A. Szlapa, T. Klemens, S. Kula, B. Machura, S. Krompiec, J. G. Matecki, A. Switlicka-Olszewska, K. Erfurt and A. Chrobok, *Org. Biomol. Chem.*, 2016, **14**, 3793.
5 B. Bonillo, R. S. Sprick and A. I. Cooper, *Chem. Mater.*, 2016, **28**, 3469.
6 X. Zhang, Z. Chi, Y. Zhang, S. Liu and J. Xu, *J. Mater. Chem. C*, 2013, **1**, 3376.
7 J. P. Lee, H. Hwang, S. Chae and J.-M. Kim, *Chem. Commun.*, 2019, **55**, 9395.
8 N. Sun, K. Su, Z. Zhou, X. Tian, Z. Jianhua, D. Chao, D. Wang, F. Lissel, X. Zhao and C. Chen, *Macromolecules*, 2019, **52**, 5131.
9 Z. Li, Y. Xie, M. Zhu, Y. Song, M. Qin and X. Hu, *Opt. Mater.*, 2019, **94**, 257.
10 D.-Y. Kim, J. Koo, S.-I. Lim and K.-U. Jeong, *Adv. Funct. Mater.*, 2018, **28**, 1707075.
11 M. Shi, J. Mack, L. Yin, X. Wang and Z. Shen, *J. Mater. Chem. C*, 2016, **4**, 7783.

12 J. Seo, J. W. Chung, J. E. Kwon and S. Y. Park, *Chem. Sci.*, 2014, **5**, 4845.
13 D.-Y. Kim, S.-A. Lee, H. Kim, S. M. Kim, N. Kim and K.-U. Jeong, *Chem. Commun.*, 2015, **51**, 11080.
14 A. Abdollahi, H. Alidaei-Sharif, H. Roghani-Mamaqani and A. Herizchi, *J. Mater. Chem. C*, 2020, **8**, 5476.
15 J. R. Talukder, H.-Y. Lin and S.-T. Wu, *Opt. Express*, 2019, **27**, 18169.
16 A. Gonzalez, E. S. Kengmana, M. V. Fonseca and G. G. D. Han, *Mater. Today Adv.*, 2020, **6**, 100058.
17 N. A. A. Rossi, E. J. Duplock, J. Meegan, D. R. T. Roberts, J. J. Murphy, M. Patel and S. J. Holder, *J. Mater. Chem.*, 2009, **19**, 7674.
18 F.-B. Meng, Y. Cui, H.-B. Chen, B.-Y. Zhang and C. Jia, *Polymer*, 2009, **50**, 1187.
19 Y. Zhang, C. Liang, H. Shang, Y. Ma and S. Jiang, *J. Mater. Chem. C*, 2013, **1**, 4472.
20 H. W. Bai, G. Wen, X. X. Huang, Z. X. Han, B. Zhong, Z. X. Hu and X. D. Zhang, *J. Eur. Ceram. Soc.*, 2011, **31**, 931.
21 D.-G. Kang, H. Ko, J. Koo, S.-I. Lim, J. S. Kim, Y.-T. Yu, C.-R. Lee, N. Kim and K.-U. Jeong, *ACS Appl. Mater. Interfaces*, 2018, **10**, 35557.
22 D.-Y. Kim, S.-A. Lee, Y.-J. Choi, S.-H. Hwang, S.-W. Kuo, C. Nah, M.-H. Lee and K.-U. Jeong, *Chem. – Eur. J.*, 2014, **20**, 5689.
23 L. Zhang, W. Yao, Y. Gao, C. Zhang and H. Yang, *Polymers*, 2018, **10**, 794.
24 D.-Y. Kim, M. Park, S.-A. Lee, S. Kim, C.-H. Hsu, N. Kim, S.-W. Kuo, T.-H. Yoon and K.-U. Jeong, *Soft Matter*, 2015, **11**, 58.
25 A. Sarkar, M. Mehra, D. Dasgupta, L. Negi and A. Saxena, *Macromolecules*, 2018, **51**, 9354.
26 W. Yao, Y. Gao, W. Yuan, B. He, H. Yu, L. Zhang, Z. Shen, W. He, Z. Yang, H. Yang and D. Yang, *J. Mater. Chem. C*, 2016, **4**, 1425.
27 H. Iino and J.-I. Hanna, *Polym. J.*, 2017, **49**, 23.
28 D.-Y. Kim, D.-G. Kang, S. Shin, T.-L. Choi and K.-U. Jeong, *Polym. Chem.*, 2016, **7**, 5304.
29 Y. Wang, H. Cui, M. Zhu, F. Qiu, J. Peng and Z. Lin, *Macromolecules*, 2017, **50**, 9674.
30 K. Ebata, Y. Hashimoto, S. Yamamoto, M. Mitsuishi, S. Nagano and J. Matsui, *Macromolecules*, 2019, **52**, 9773.
31 S. Liang, Y. Xu, C. Li, J. Li, D. Wang and W. Li, *Polym. Chem.*, 2019, **10**, 4584.
32 Y. Yuan, J. Li, L. He, Y. Liu and H. Zhang, *J. Mater. Chem. C*, 2018, **6**, 7119.
33 Y. Ma, M. Cametti, Z. Dzolic and S. Jiang, *J. Mater. Chem. C*, 2016, **4**, 10786.
34 M. Martinez-Abadia, S. Varghese, R. Gimenez and M. B. Ros, *J. Mater. Chem. C*, 2016, **4**, 2886.
35 Z. Ding, Y. Ma, H. Shang, H. Zhang and S. Jiang, *Chem. – Eur. J.*, 2019, **25**, 315.
36 L. Zhu, C. Y. Ang, X. Li, K. T. Nguyen, S. Y. Tan, H. Agren and Y. Zhao, *Adv. Mater.*, 2012, **24**, 4020.
37 Y. Zhu, M. Zheng, Y. Tu and X.-F. Chen, *Macromolecules*, 2018, **51**, 3487.
38 S.-W. Oh, S.-H. Kim and T.-H. Yoon, *J. Mater. Chem. C*, 2018, **6**, 6520.
39 K. V. Deriabin, E. K. Lobanovskaia, A. S. Novikov and R. M. Islamova, *Org. Biomol. Chem.*, 2019, **17**, 5545.
40 K. V. Deriabin, E. K. Lobanovskaia, S. O. Kirichenko, M. N. Barshutina, P. E. Musienko and R. M. Islamova, *Appl. Organomet. Chem.*, 2020, **34**, e5300.
41 J. Koo, S.-I. Lim, S. H. Lee, J. S. Kim, Y.-T. Yu, C.-R. Lee, D.-Y. Kim and K.-U. Jeong, *Macromolecules*, 2019, **52**, 1739.
42 Z. Wen, M. K. McBride, X. Zhang, X. Han, A. M. Martinez, R. Shao, C. Zhu, R. Visvanathan, N. A. Clark, Y. Wang, K. Yang and C. N. Bowman, *Macromolecules*, 2018, **51**, 5812.
43 M. O. Saed, R. H. Volpe, N. A. Traugutt, R. Visvanathan, N. A. Clark and C. M. Yakacki, *Soft Matter*, 2017, **13**, 7537.
44 H. Wang, W. Deng, H. Wu, A. Pi, J. Li and F. Huang, *Def. Technol.*, 2019, **15**, 875.
45 T. Han, L. Liu, D. Wang, J. Yang and B. Z. Tang, *Macromol. Rapid Commun.*, 2020, 2000311.
46 A. Pucci, *Sensors*, 2019, **19**, 4969.
47 P. Im, D.-G. Kang, D.-Y. Kim, Y.-J. Choi, W.-J. Yoon, M.-H. Lee, I.-H. Lee, C.-R. Lee and K.-U. Jeong, *ACS Appl. Mater. Interfaces*, 2016, **8**, 762.
48 D. Shi, W.-Y. Chang, X.-K. Ren, S. Yang and E.-Q. Chen, *Polym. Chem.*, 2020, **11**, 4749.
49 J. Geng, X. Zhao, E. Zhou, G. Li, J. W. Y. Lam and B. Z. Tang, *Polymer*, 2003, **44**, 8095.
50 R. He, E. Oh, Y. Ye, P. Wen, K.-U. Jeong, S. H. Lee, X.-D. Li and M.-H. Lee, *Polymer*, 2019, **176**, 51.
51 V. K. Baliyan, V. Kumar, J. Kim and S.-W. Kang, *Opt. Mater. Express*, 2016, **6**, 2956.